Electrocatalysis

Deutsche Ausgabe: DOI: 10.1002/ange.201502577
Internationale Ausgabe: DOI: 10.1002/anie.201502577

One-Step Synthesis of Self-Supported Nickel Phosphide Nanosheet Array Cathodes for Efficient Electrocatalytic Hydrogen Generation**

*Xiaoguang Wang, Yury V. Kolen'ko, Xiao-Qing Bao, Kirill Kovnir, and Lifeng Liu**

Abstract: *Nickel phosphide is an emerging low-cost, earth-abundant catalyst that can efficiently reduce water to generate hydrogen. However, the synthesis of nickel phosphide catalysts usually involves multiple steps and is laborious. Herein, a convenient and straightforward approach to the synthesis of a three-dimensional (3D) self-supported biphasic Ni_5P_4-Ni_2P nanosheet (NS) array cathode is presented, which is obtained by direct phosphorization of commercially available nickel foam using phosphorus vapor. The synthesized 3D Ni_5P_4-Ni_2P-NS array cathode exhibits outstanding electrocatalytic activity and long-term durability toward the hydrogen evolution reaction (HER) in acidic medium. The fabrication procedure reported here is scalable, showing substantial promise for use in water electrolysis. More importantly, the approach can be readily extended to synthesize other self-supported transition metal phosphide HER cathodes.*

Hydrogen, H_2, has been proposed to be a clean and carbon-neutral next-generation energy carrier. Globally, H_2 is mainly produced by steam reforming, a process which is not only environmentally unfriendly, but also consumes nonrenewable fossil fuels. Compared with steam reforming, water electrolysis represents a cleaner and more sustainable approach to H_2 generation, but is underdeveloped. To deploy electrolyzers on a large scale and to make the electrolyzed H_2 fuel economically competitive, it is important to develop inexpensive, earth-abundant electrocatalysts to promote the hydrogen evolution reaction (HER). This is also a pressing need for solar-driven photoelectrochemical water splitting.[1] To this end, many efforts have already been made to develop HER catalysts containing nonnoble metals, such as NiMo,[2] MoS_2,[3] MoS_x,[4] MoC,[5] WS_2,[6] WC,[7] Ni-P,[8] Co-P,[9] Fe-P,[10] MoP,[11] and WP[12] to replace the commonly used precious Pt catalysts, among which Ni-P has emerged as a new earth-abundant HER catalyst since 2013.[8a] In the past two years, a variety of Ni-P HER catalysts with different stoichiometries like Ni_2P,[8a,b,d,i,j] $N_{12}P_5$,[8c,e,h] NiP_2,[8g] Ni_5P_4,[8h] and morphologies including nanoparticles,[8a–d,h] nanorods,[8f,j] nanosheets,[8g] and peapods,[8i] have been reported, and their catalytic performance toward HER was carefully investigated.

According to the literature published so far, there are generally two ways to prepare HER cathodes based on the newly developed transition metal phosphide (TMP) catalysts including Ni-P: one method involves the synthesis of TMP nanocatalysts by solvothermal reactions, followed by their immobilization on a conductive support such as a Ti plate[8a,c,9a,e,10b,11c,12a] or glassy carbon[8b,h,10c,11a,b] using Nafion or a polymeric binder; the other way aims to develop binder-free cathodes, which can be realized by first growing transition metal oxide/hydroxide (TMO/TMOH) nanostructures through hydrothermal processing[9b,10a] or electrodeposition[9c] on a current collector, for example, a Ti sheet,[8d,9c,10a] carbon cloth,[8g,9b] or copper foam,[13] then converting TMO/TMOH into TMP through a low-temperature phosphidation reaction.

Here, we report a very simple and straightforward method to fabricate self-supported biphasic Ni_5P_4-Ni_2P nanosheet (NS) array cathodes for HER. The cathode is obtained by direct phosphorization of commercially available Ni foam using phosphorus vapor without complicated chemical reactions and posttreatment steps involved. Moreover, the as-obtained electrode is self-supported and can be directly used as a cathode for HER. We demonstrate that the self-supported Ni_5P_4-Ni_2P-NS array cathode exhibits an HER onset potential (η, the potential at which the cathodic current density is 1 mA cm^{-2}) of −54 mV, a Tafel slope of 79.1 mV dec^{-1}, and an exchange current density of 0.116 mA cm^{-2}. Overpotentials of merely 120, 140, and 200 mV are needed to reach cathodic current densities of 10, 20, and 100 mA cm^{-2}, respectively. Furthermore, the cathode can sustain for up to 72 h at a cathodic current density of 10 mA cm^{-2} with little increase in the overpotential, showing good long-term durability toward HER.

In our experiments, a piece of Ni foam (ca. 0.3 g, 5 mmol) was loaded together with about 1 g (32 mmol) of red phosphorus in a tube furnace, and heated to 400, 500, 600, or 800 °C for 6 h in a flow of N_2 (99.999 %, see the Supporting Information for details). Scanning electron microscopy (SEM) examination reveals that the sheet-like morphology only appears at 400 and 500 °C (Figure S1a and S1b). Electrochemical measurements show that the sample phosphorized at 500 °C is the most active toward HER (Figure S2). Therefore, unless specified otherwise, all data presented here were acquired with the sample phosphorized at 500 °C.

Figure 1a is the X-ray diffraction (XRD) pattern of the as-synthesized Ni_5P_4-Ni_2P-NS array cathode (i.e., 500 °C, 6 h),

[*] Dr. X. G. Wang, Dr. Y. V. Kolen'ko, Dr. X. Q. Bao, Dr. L. F. Liu
International Iberian Nanotechnology Laboratory (INL)
Av. Mestre Jose Veiga, 4715-330 Braga (Portugal)
E-mail: Lifeng.Liu@inl.int
Prof. Dr. K. Kovnir
Department of Chemistry, University of California, Davis
Davis, CA 95616 (USA)

[**] X.G.W. and L.F.L. acknowledge financial support of Marie-Curie COFUND programme (NanoTrainforGrowth). L.F.L. acknowledges financial support of the FCT Investigator grant (No. IF/01595/2014). Y.V.K. thanks Dr. L. M. Salonen and Prof. P. P. Freitas for helpful discussions.

Supporting information for this article is available on the WWW under http://dx.doi.org/10.1002/anie.201502577.

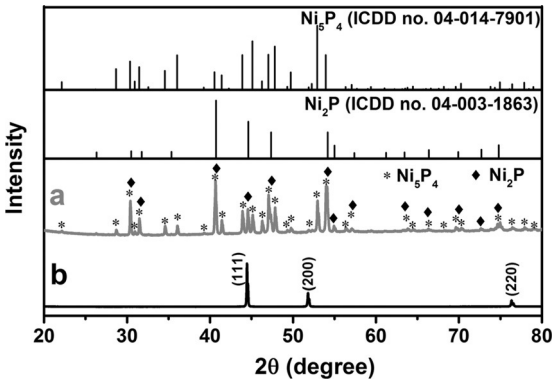

Figure 1. XRD patterns of a) the as-synthesized Ni_5P_4-Ni_2P-NS array cathode, and b) a pristine Ni foam for comparison. The standard powder X-ray diffraction patterns of Ni_5P_4 and Ni_2P are also given for reference.

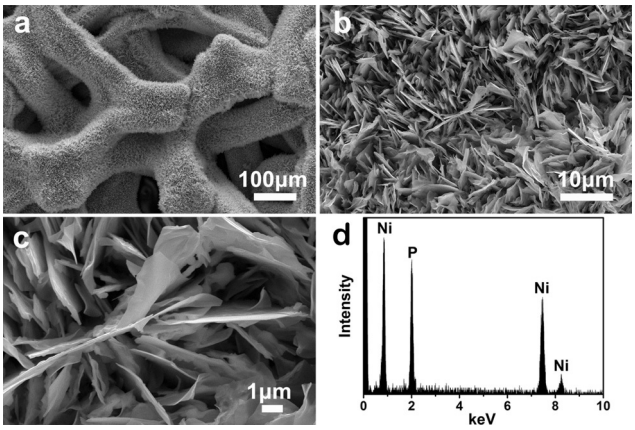

Figure 2. a) Low- and b,c) high-magnification SEM images of Ni_5P_4-Ni_2P-NS array cathode. d) EDX spectrum.

showing that the sample is composed of a mixture of hexagonal Ni_5P_4 (ICDD no. 04-014-7901) and Ni_2P (ICDD no. 04-003-1863), in which Ni_5P_4 is the major component accounting for ca. 80 wt% (Figure S3). Notably, the intensity of the diffraction peaks from metallic Ni becomes fairly weak after phosphorization, indicating an almost complete conversion of Ni to nickel phosphide. This is also confirmed by SEM elemental mapping over the cross-section of the ligaments, which shows that P is present over the entire ligaments (Figure S4). The areal density of the as-obtained Ni_5P_4-Ni_2P-NS electrode is measured to be 68.2 mg cm^{-2}.

After the phosphorization treatment, the original bright silver color of the pristine Ni foam turned to black (Figure S5a), and the foam became brittle. Upon inspection of the foam surface using scanning electron microscopy (SEM), it was found that the macroporous morphology remains unchanged, however, a burr-like skin appears on the entire surface of the foam (Figures 2a and S5c). A closer look reveals that the ligament surface is uniformly covered with a high-density array of vertically-aligned NSs (Figure 2b and c), the thickness of which ranges from several tens to one hundred nanometers. The corresponding energy-dispersive X-ray (EDX) spectrum verifies that these NSs consist exclusively of Ni and P (Figure 2d). No peaks from other elements were observed. Moreover, SEM-EDX mapping shows that Ni and P are uniformly distributed over the ligament surface (Figure S6).

Reaction of phosphorus vapor with metal powder is a common way of producing metal phosphides in solid-state chemistry.[14] For example, Ni_5P_4 was produced by reaction of Ni powder and phosphorus in evacuated silica ampoules at 800–900 °C.[15] Similar reaction may occur in the liquid phase either in molten metal fluxes or under solvothermal conditions.[8j,16] We hypothesized that the Ni_5P_4-Ni_2P-NS array forms through a direct topotactic redox reaction between Ni foam and P vapor, which is driven by the transfer of electrons from the electropositive Ni metal to the electronegative P.[16] Given the macroporous features of the Ni foam that allow P vapor to readily access the foam surface, the formation of NSs should start simultaneously at all surface sites through a short nucleation step. This will then proceed by kinetically controlled growth of primary crystallites along favorable axis of the hexagonal Ni_5P_4 or Ni_2P. Simultaneous nucleation and homogeneous supply of precursor P vapor finally lead to the uniform growth of vertically aligned NSs over the entire surface of the foam.

Figure 3a shows a representative low-magnification transmission electron microscopy (TEM) image of a single NS,

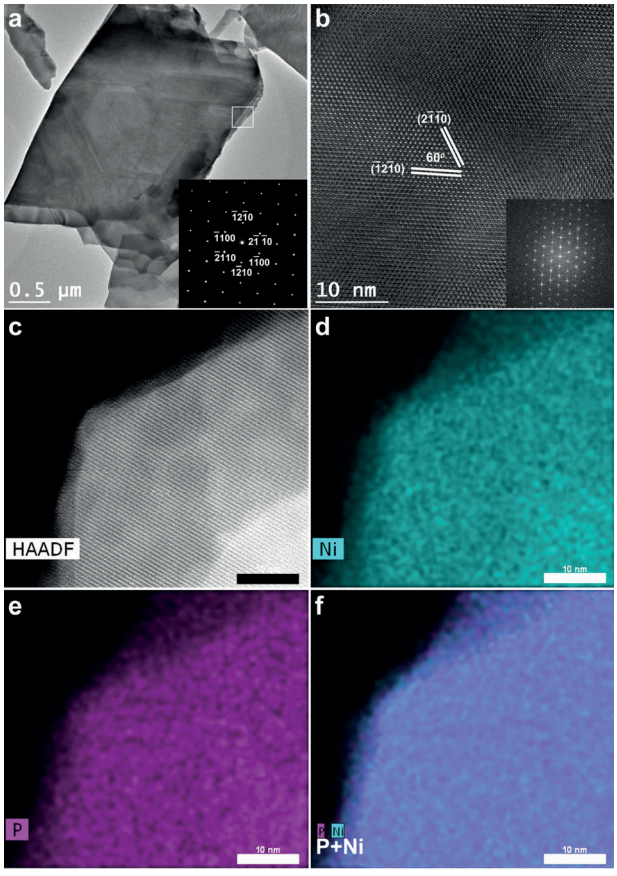

Figure 3. a) TEM and b) HRTEM images of a single NS. Corresponding SAED and FFT-ED patterns are shown as insets. c) HAADF-STEM image together with elemental maps for d) Ni, e) P, and f) P + Ni. Scale bars in c–f: 10 nm.

confirming its plate-like feature. Observed selected-area electron diffraction (SAED) over this NS displays a well-defined spotted pattern corresponding to the diffraction along the [0001] zone axis of the Ni_5P_4 hexagonal structure, indicative of the single-crystalline nature of this NS (Figure 3a, inset). This is further corroborated by high-resolution TEM (HRTEM) investigation (Figure 3b), in which well-resolved crystal lattices with an interplanar spacing of 0.587 nm can be clearly distinguished, corresponding to the distance of $(2\bar{1}\bar{1}0)$ and $(\bar{1}2\bar{1}0)$ crystal planes of the hexagonal Ni_5P_4.[15] Moreover, the interplanar angle is measured to be 60°. These results prove that the NS under investigation consists exclusively of Ni_5P_4. Furthermore, the fast Fourier transformation (FFT) of this HRTEM image shows a pattern pretty similar to the SAED pattern, indicating that the local microstructure of the NS perfectly matches the overall crystal structure. To further examine the composition of the NS, high-angle annular dark-field scanning TEM (HAADF-STEM) was performed. Figure 3c–f show a HAADF-STEM image and the corresponding elemental maps of Ni, P, and Ni + P, which confirm that both Ni and P are uniformly distributed over the NS, and no segregation was discernible.

Figure 4a shows the polarization curve of the Ni_5P_4-Ni_2P-NS array cathode, measured in N_2-saturated 0.5 M H_2SO_4 with a scan rate of 10 mV s^{-1}. A pristine Ni foam, a Pt sheet, and commercial Pt/C catalysts were also examined for comparison. All polarization curves are *iR*-corrected (i.e., electrolyte resistance compensated, see SI for details). The Pt-based catalysts including Pt sheet and 20% Pt/C, as expected, reveal the best HER activity with a near-zero overpotential. The Ni_5P_4-Ni_2P-NS array exhibits an HER onset potential as small as −54 mV, which is only slightly lower than that of Pt electrodes. Further increase in the cathodic potential leads to a sharp rise in the cathodic current. The Ni_5P_4-Ni_2P-NS cathode can offer cathodic current densities of 10, 20, and 100 mA cm^{-2} for HER at overpotentials of 120 (η_{10}), 140 (η_{20}), and 200 mV (η_{100}), respectively, the performance of which favorably compares to that of many previously reported nonprecious HER catalysts measured in acidic solutions, including Mo- and W-based catalysts as well as some recently developed TMPs (Table S1). In contrast, the pristine Ni foam only shows negligible cathodic current in the potential range of −300 to 0 mV versus RHE. Figure 4b presents the Tafel plots of the fabricated Ni_5P_4-Ni_2P-NS array cathode, a pristine Ni foam, a Pt sheet, and commercial Pt/C. A linear fit using the Tafel equation, $\eta = a + b\log(j)$ (in which η is the overpotential, a the Tafel constant, b the Tafel slope, and j the current density), yields apparent Tafel slopes of 79.1, 190.5, 64.7, and 31.6 mV dec^{-1} for the Ni_5P_4-Ni_2P-NS array, pristine Ni foam, Pt sheet, and Pt/C, respectively. The apparent Tafel slope of the Ni_5P_4-Ni_2P-NS array is larger than that of the Pt-based catalysts, but comparable to that of Ni_2P nanoparticles reported by Feng et al. (87 mV dec^{-1} at η = 60–140 mV)[8b] and Popczun et al. (81 mV dec^{-1} at η = 150–200 mV)[8a] and smaller than that of some previously reported nonnoble metal catalysts like bulk MoS_2 (94 mV dec^{-1}),[3d] Mo_2C nanocrystals (110–235 mV dec^{-1}),[17a] and $MoSe_2$/RGO (101 mV dec^{-1}).[17b] The slope falls within the range of 40–120 mV dec^{-1}, suggesting that the HER taking place on the Ni_5P_4-Ni_2P-NS surface would follow a Volmer–Heyrovsky mechanism, and that the rate of the discharge step would be consistent with that of the desorption step.[8e,9e] By extrapolating the Tafel plot to an overpotential of 0 V, the exchange current density (j_0) of the HER on Ni_5P_4-Ni_2P-NSs is obtained, being 0.116 mA cm^{-2}, outperforming that of

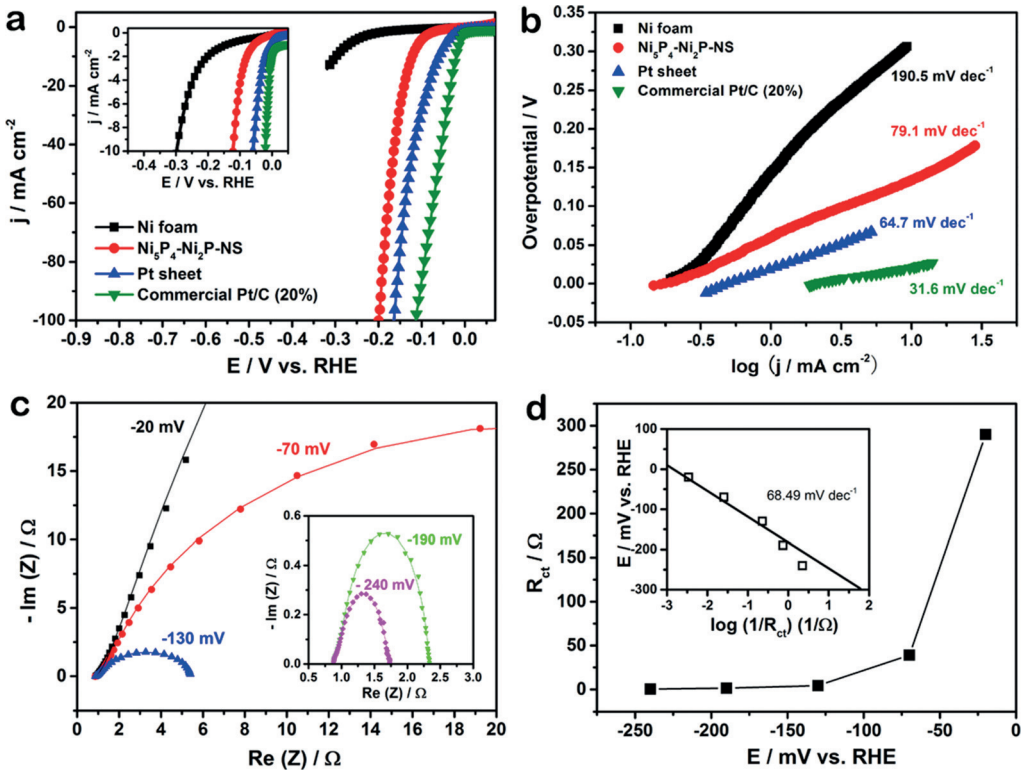

Figure 4. a) Polarization (LSV) curves, and b) Tafel plots of the Ni_5P_4-Ni_2P-NS array, pristine Ni foam, Pt sheet, and commercial Pt/C (20%) catalysts. c) Nyquist plots of the Ni_5P_4-Ni_2P-NS array cathode measured at different overpotentials in the frequency range of 10^5–0.05 Hz. d) Dependence of the charge-transfer resistance (R_{ct}) on the overpotential. Inset: overpotential versus $\log(R_{ct}^{-1})$. Scatters: experimental data; line: fitting curves. All measurements were carried out in N_2-saturated 0.5 M H_2SO_4 solution at room temperature. Scan rate in (a): 10 mV s^{-1}.

many transition metal sulfides and phosphides reported in the literature, such as MoS_2,[3c–f] MoP,[11a,b] and CoP[9f] (Table S1).

The outstanding HER electrocatalytic activity of the Ni_5P_4-Ni_2P-NS arrays can be attributed, on the one hand, to the unique topology of the electrode that comprises 3D microporous skeleton covered with high-density upright NSs, which not only maximizes the number of exposed active sites, but also facilitates the diffusion of electrolyte and the release of generated gas bubbles. On the other hand, the presence of a large fraction of Ni_5P_4 and the synergistic effect between Ni_5P_4 and Ni_2P phases may contribute to the excellent activity, given the fact that the catalytic activity of the biphasic Ni_5P_4-Ni_2P-NS array is higher than that of the phase-pure Ni_2P-NS array prepared by phosphorization at 400 °C (Figures S2 and S7). The superior electrocatalytic activity of Ni_5P_4 over that of Ni_2P was recently reported,[8h] and can be ascribed to the high positive charge of Ni and a strong ensemble effect of P in Ni_5P_4.

To explore the HER electrode kinetics, electrochemical impedance spectroscopy (EIS) investigations on the Ni_5P_4-Ni_2P-NS array cathode were performed. The EIS experiments were carried out at different applied overpotentials, as illustrated by the Nyquist plots shown in Figure 4c. Experimental data were fitted using an equivalent circuit consisting of a resistor (R_s) in series with two parallel combinations of a resistor (R_1, R_{ct}) and a constant phase element (CPE_1, CPE_2),[3g,8b] in which R_s represents the ohmic resistance arising from the electrolyte and all contacts, the time constant R_1-CPE_1 may relate to the interfacial resistance resulting from the electron transport between the Ni_5P_4-Ni_2P-NSs and the porous skeleton underneath, and R_{ct}-CPE_2 reflects the charge transfer resistance (R_{ct}) at the interface between the NSs and the electrolyte. (Figure S8 and Table S2). It is generally accepted that a small R_{ct} gives rise to fast charge transfer kinetics. R_{ct} of the Ni_5P_4-Ni_2P-NS cathode as a function of the overpotential applied is plotted in Figure 4d, in which it is clearly seen that R_{ct} is potential-dependent. At an overpotential of 20 mV the R_{ct} was fitted to be 289.9 Ω; it sharply decreases to 4.4 Ω at −130 mV, and down to merely 0.4 Ω at −240 mV (Table S2), indicating that the charge-transfer kinetics is significantly accelerated upon increasing the overpotential. The Tafel plot can also be derived from the plot of η versus log (R_{ct}^{-1}) (Figure 4d, inset), which is 68.49 mV dec^{-1}, slightly smaller than that extracted from the polarization curve (i.e., 79.1 mV dec^{-1}). This can be explained by the fact that the Tafel slope obtained from Figure 4d only reflects the charge-transfer kinetics without considering the contributions from the catalyst resistance,[18] unlike those derived from polarization curves (i.e., Figure 4b).

Stability and durability are important indicators for HER catalysts, and were evaluated by accelerated degradation test (ADT) and chronopotentiometry. The ADT was performed by sweeping the potential in a range of −200–60 mV versus RHE at a rate of 50 mV s^{-1}. Figure 5 shows the polarization curves of the Ni_5P_4-Ni_2P-NS array cathode before and after ADT for 1000 continuous cycles. The electrode shows only a slight degradation after 1000 cycles of ADT, with an overpotential increase of merely 18 and 21 mV to achieve current densities of 10 and 100 mA cm^{-2}, respectively. The

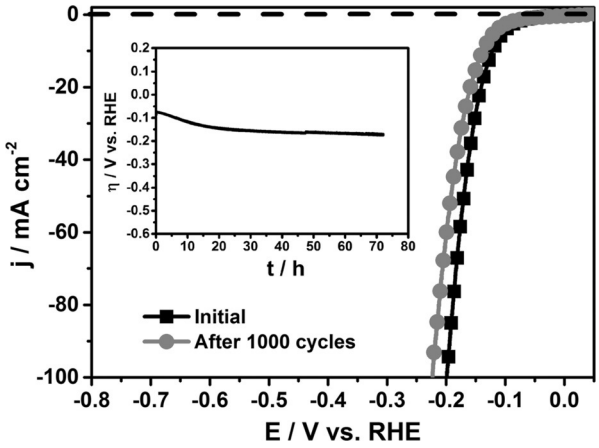

Figure 5. Polarization curves of the Ni_5P_4-Ni_2P-NS array cathode measured before and after ADT for 1000 continuous cycles. Scan rate: 10 mV s^{-1}. Inset: η–t profile recorded at a constant cathodic current of 10 mA cm^{-2}. All measurements were performed in N_2-saturated 0.5 M H_2SO_4 solution at room temperature.

stability of the Ni_5P_4-Ni_2P-NS array is much better than that of the Ni_2P nanoparticles supported on Ti electrode reported previously.[8a] The durability of the Ni_5P_4-Ni_2P-NS array cathode was examined by electrolysis in N_2-saturated 0.5 M H_2SO_4 solution at a fixed cathodic current density of 10 mA cm^{-2} over three days (Figure 5, inset). The overpotential slowly increases within the initial 20 h from 80 mV to 144 mV, which presumably results from partial blockage of some active sites by reaction intermediates and/or local dissolution of the NSs, as revealed by inductively coupled plasma optical emission spectroscopy (ICP-OES) analysis (Table S3). Afterwards, it begins to level off at this overpotential to provide a constant cathodic current of 10 mA cm^{-2} for HER up to 72 h, showing excellent durability. It is worth mentioning that the sheet-like morphology of the Ni_5P_4-Ni_2P-NS array remains unchanged after extended stability and durability tests (Figure S9a and S9b). Moreover, EDX analysis shows that no other elements exist in the tested electrode except Ni and P (Figure S9c), and both Ni and P are uniformly distributed over the porous framework (Figure S10). Furthermore, quantitative XRD phase analysis demonstrates that the weight ratio of Ni_5P_4 over Ni_2P varies only slightly within an accepted error range (Figure S11). All these results from morphological and compositional characterization manifest that the overall porous framework and individual NSs are highly acid-stable.

In summary, a one-step route for the synthesis of self-supported three-dimensional Ni_5P_4-Ni_2P nanosheet arrays is reported. The fabricated Ni_5P_4-Ni_2P nanosheet array can be directly utilized as a cathode for electrocatalytic hydrogen generation, which shows outstanding catalytic activity and excellent long-term stability and durability in acidic medium. Compared with the multistep synthetic methods reported in the literature, direct phosphorization of nickel foams using phosphoric vapor offers a very simple and straightforward approach to the fabrication of self-supported low-cost HER cathodes, which can be readily up-scaled due to the commercial availability and cost-effectiveness of nickel foam as well

as the simplicity of the phosphorization process. The novel method can be easily extended to synthesize other porous transition metal phosphide cathodes using the corresponding transition metal foam as the starting materials. The self-supported three-dimensional nickel phosphide nanosheet array electrodes reported in this work hold substantial promise for use as low-cost cathodes for efficient water electrolysis.

Keywords: electrocatalysis · heterogeneous catalysis · hydrogen evolution · nanostructures · nickel phosphide

How to cite: *Angew. Chem. Int. Ed.* **2015**, *54*, 8188–8192
Angew. Chem. **2015**, *127*, 8306–8310

[1] a) M. G. Walter, E. L. Warren, J. R. McKone, S. W. Boettcher, Q. X. Mi, E. A. Santori, N. S. Lewis, *Chem. Rev.* **2010**, *110*, 6446–6473; b) D. Merki, X. L. Hu, *Energy Environ. Sci.* **2011**, *4*, 3878–3888.

[2] L. Birry, A. Lasia, *J. Appl. Electrochem.* **2004**, *34*, 735–749.

[3] a) T. F. Jaramillo, K. P. Jørgensen, J. Bonde, J. H. Nielsen, S. Horch, I. Chorkendorff, *Science* **2007**, *317*, 100–102; b) Y. G. Li, H. L. Wang, L. M. Xie, Y. Y. Liang, G. S. Hong, H. J. Dai, *J. Am. Chem. Soc.* **2011**, *133*, 7296–7299; c) J. Xie, H. Zhang, S. Li, R. Wang, X. Sun, M. Zhou, J. Zhou, X. W. Lou, Y. Xie, *Adv. Mater.* **2013**, *25*, 5807–5813; d) T. Y. Wang, L. Liu, Z. W. Zhu, P. Papakonstantinou, J. B. Hu, M. Li, *Energy Environ. Sci.* **2013**, *6*, 625–633; e) D. Z. Wang, Z. Pan, Z. Z. Wu, Z. P. Wang, Z. H. Liu, *J. Power Sources* **2014**, *264*, 229–234; f) T. Y. Chen, Y. H. Chang, C. L. Hsu, K. H. Wei, C. Y. Chiang, L. J. Li, *Int. J. Hydrogen Energy* **2013**, *38*, 12302–12309; g) L. Liao, S. N. Wang, J. J. Xiao, X. J. Bian, Y. H. Zhang, M. D. Scanlon, X. L. Hu, Y. Tang, B. H. Liu, H. H. Girault, *Energy Environ. Sci.* **2014**, *7*, 387–392.

[4] a) D. Merki, S. Fierro, H. Vrubel, X. L. Hu, *Chem. Sci.* **2011**, *2*, 1262–1267; b) A. B. Laursen, P. C. K. Vesborg, I. Chorkendorff, *Chem. Commun.* **2013**, *49*, 4965–4967.

[5] C. Wan, Y. N. Regmi, B. M. Leonard, *Angew. Chem. Int. Ed.* **2014**, *53*, 6407–6410; *Angew. Chem.* **2014**, *126*, 6525–6528.

[6] D. Voiry, H. Yamaguchi, J. W. Li, R. Silva, D. C. B. Alves, T. Fujita, M. W. Chen, T. Asefa, V. B. Shenoy, G. Eda, M. Chhowalla, *Nat. Mater.* **2013**, *12*, 850–855.

[7] F. Harnisch, G. Sievers, U. Schröder, *Appl. Catal. B* **2009**, *89*, 455–458.

[8] a) E. J. Popczun, J. R. McKone, C. G. Read, A. J. Biacchi, A. M. Wiltrout, N. S. Lewis, R. E. Schaak, *J. Am. Chem. Soc.* **2013**, *135*, 9267–9270; b) L. G. Feng, H. Vrubel, M. Bensimon, X. L. Hu, *Phys. Chem. Chem. Phys.* **2014**, *16*, 5917–5921; c) Z. P. Huang, Z. B. Chen, Z. Z. Chen, C. C. Lv, H. Meng, C. Zhang, *ACS Nano* **2014**, *8*, 8121–8129; d) Z. H. Pu, Q. Liu, C. Tang, A. M. Asiri, X. P. Sun, *Nanoscale* **2014**, *6*, 11031–11034; e) A. R. J. Kucernak, V. N. N. Sundaram, *J. Mater. Chem. A* **2014**, *2*, 17435–17445; f) A. L. Lu, Y. Z. Chen, H. Y. Li, A. Dowd, M. B. Cortie, Q. S. Xie, H. Z. Guo, Q. Q. Qi, D. L. Peng, *Int. J. Hydrogen Energy* **2014**, *39*, 18919–18928; g) P. Jiang, Q. Liu, X. P. Sun, *Nanoscale* **2014**, *6*, 13440–13445; h) Y. Pan, Y. R. Liu, J. C. Zhao, K. Yang, J. L. Liang, D. D. Liu, W. H. Hu, D. P. Liu, Y. Q. Liu, C. G. Liu, *J. Mater. Chem. A* **2015**, *3*, 1656–1665; i) Y. J. Bai, H. J. Zhang, X. Li, L. Liu, H. T. Xu, H. J. Qiu, Y. Wang, *Nanoscale* **2015**, *7*, 1446–1453; j) X. G. Wang, Y. V. Kolen'ko, L. F. Liu, *Chem. Commun.* **2015**, *51*, 6738–6741.

[9] a) E. J. Popczun, C. G. Read, C. W. Roske, N. S. Lewis, R. E. Schaak, *Angew. Chem. Int. Ed.* **2014**, *53*, 5427–5430; *Angew. Chem.* **2014**, *126*, 5531–5534; b) J. Q. Tian, Q. Liu, A. M. Asiri, X. P. Sun, *J. Am. Chem. Soc.* **2014**, *136*, 7587–7590; c) Z. H. Pu, Q. Liu, P. Jiang, A. M. Asiri, A. Y. Obaid, X. P. Sun, *Chem. Mater.* **2014**, *26*, 4326–4329; d) H. F. Du, Q. Liu, N. Y. Cheng, A. M. Asiri, X. P. Sun, C. M. Li, *J. Mater. Chem. A* **2014**, *2*, 14812–14816; e) Z. P. Huang, Z. Z. Chen, Z. B. Chen, C. C. Lv, M. G. Humphrey, C. Zhang, *Nano Energy* **2014**, *9*, 373–382; f) Q. Liu, J. Q. Tian, W. Cui, P. Jiang, N. Y. Cheng, A. M. Asiri, X. P. Sun, *Angew. Chem. Int. Ed.* **2014**, *53*, 6710–6714; *Angew. Chem.* **2014**, *126*, 6828–6832.

[10] a) P. Jiang, Q. Liu, Y. H. Liang, J. Q. Tian, A. M. Asiri, X. P. Sun, *Angew. Chem. Int. Ed.* **2014**, *53*, 12855–12859; *Angew. Chem.* **2014**, *126*, 13069–13073; b) J. F. Callejas, J. M. McEnaney, C. G. Read, J. C. Crompton, A. J. Biacchi, E. J. Popczun, T. R. Gordon, N. S. Lewis, R. E. Schaak, *ACS Nano* **2014**, *8*, 11101–11107; c) Z. P. Huang, C. C. Lv, Z. Z. Chen, Z. B. Chen, F. Tian, C. Zhang, *Nano Energy* **2015**, *12*, 666–674; d) Y. Xu, R. Wu, J. F. Zhang, Y. M. Shi, B. Zhang, *Chem. Commun.* **2013**, *49*, 6656–6658.

[11] a) P. Xiao, M. A. Sk, L. Thia, X. M. Ge, R. J. Lim, J. Y. Wang, K. H. Lim, X. Wang, *Energy Environ. Sci.* **2014**, *7*, 2624–2629; b) Z. C. Xing, Q. Liu, A. M. Asiri, X. P. Sun, *Adv. Mater.* **2014**, *26*, 5702–5707; c) J. M. McEnaney, J. C. Crompton, J. F. Callejas, E. J. Popczun, A. J. Biacchi, N. S. Lewis, R. E. Schaak, *Chem. Mater.* **2014**, *26*, 4826–4831.

[12] a) J. M. McEnaney, J. C. Crompton, J. F. Callejas, E. J. Popczun, C. G. Read, N. S. Lewis, R. E. Schaak, *Chem. Commun.* **2014**, *50*, 11026–11028; b) Z. C. Xing, Q. Liu, A. M. Asiri, X. P. Sun, *ACS Catal.* **2015**, *5*, 145–149.

[13] J. Q. Tian, Q. Liu, N. Y. Cheng, A. M. Asiri, X. P. Sun, *Angew. Chem. Int. Ed.* **2014**, *53*, 9577–9581; *Angew. Chem.* **2014**, *126*, 9731–9735.

[14] a) H. G. von Schnering, W. Hoenle, *Chem. Rev.* **1988**, *88*, 243–273; b) M. M. Shatruk, K. Kovnir, A. V. Shevelkov, B. A. Popovkin, *Angew. Chem. Int. Ed.* **2000**, *39*, 2508–2509; *Angew. Chem.* **2000**, *112*, 2561–2562.

[15] M. Elfström, *Acta Chem. Scand.* **1965**, *19*, 1694–1704.

[16] a) M. G. Kanatzidis, R. Pottgen, W. Jeitschko, *Angew. Chem. Int. Ed.* **2005**, *44*, 6996–7023; *Angew. Chem.* **2005**, *117*, 7156–7184; b) Y. Xie, H. L. Su, X. F. Qian, X. M. Liu, Y. T. Qian, *J. Solid State Chem.* **2000**, *149*, 88–91; c) K. A. Kovnir, Y. V. Kolen'ko, S. Ray, J. W. Li, T. Watanabe, M. Itoh, M. Yoshimura, A. V. Shevelkov, *J. Solid State Chem.* **2006**, *179*, 3756–3762; d) K. Kovnir, Y. V. Kolen'ko, A. I. Baranov, I. S. Neira, A. V. Sobolev, M. Yoshimura, I. A. Presniakov, A. V. Shevelkov, *J. Solid State Chem.* **2009**, *182*, 630–639.

[17] a) N. S. Alhajri, D. H. Anjum, K. Takanabe, *J. Mater. Chem. A* **2014**, *2*, 10548–10556; b) H. Tang, K. Dou, C. C. Kaun, Q. Kuang, S. Yang, *J. Mater. Chem. A* **2014**, *2*, 360–364.

[18] H. Vrubel, T. Moehl, M. Grätzel, X. L. Hu, *Chem. Commun.* **2013**, *49*, 8985–8987.

Received: March 19, 2015
Published online: June 1, 2015

